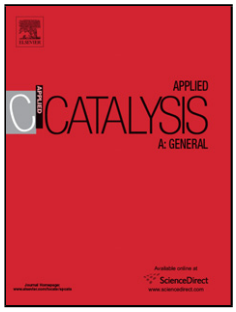

Title: The influence of alumina phases on the performance of Pd/Al_2O_3 catalyst in selective hydrogenation of benzonitrile to benzylamine

Authors: Chengyong Dai, Yonggang Li, Chunli Ning, Wenxiang Zhang, Xueguang Wang, Chunlei Zhang

PII: S0926-860X(17)30342-3
DOI: http://dx.doi.org/doi:10.1016/j.apcata.2017.07.032
Reference: APCATA 16337

To appear in: *Applied Catalysis A: General*

Received date: 4-5-2017
Revised date: 15-7-2017
Accepted date: 21-7-2017

Please cite this article as: Chengyong Dai, Yonggang Li, Chunli Ning, Wenxiang Zhang, Xueguang Wang, Chunlei Zhang, The influence of alumina phases on the performance of Pd/Al2O3 catalyst in selective hydrogenation of benzonitrile to benzylamine, Applied Catalysis A, Generalhttp://dx.doi.org/10.1016/j.apcata.2017.07.032

Highlights

- Performance of various Pd/Al_2O_3 are compared for benzonitrile hydrogenation
- Catalytic activity of Pd/Al_2O_3 relies on H_2 transmission rate
- Both $Pd/\gamma\text{-}Al_2O_3$ and $Pd/\eta\text{-}Al_2O_3$ achieve a high benzylamine yield of ca. 90%
- Formation of dibenzylamine has a close relation with Pd dispersion

The influence of alumina phases on the performance of Pd/Al_2O_3 catalyst in selective hydrogenation of benzonitrile to benzylamine

Graphical abstract

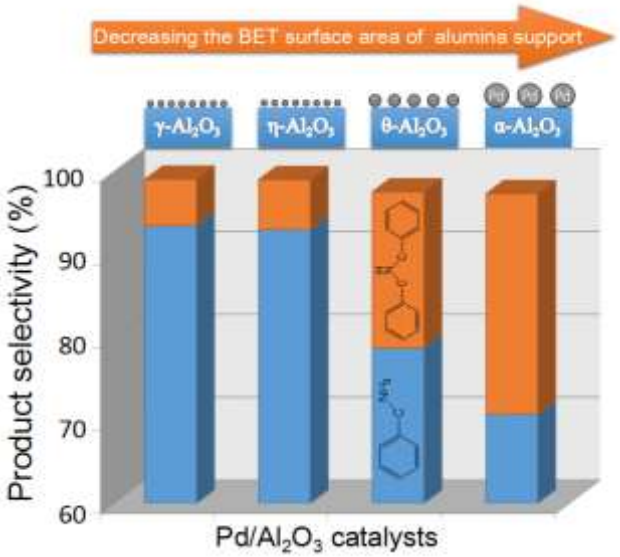

The influence of alumina phases on the performance of Pd/Al_2O_3 catalyst in selective hydrogenation of benzonitrile to benzylamine

Chengyong Dai[a, b], Yonggang Li[b], Chunli Ning[b], Wenxiang Zhang[b], Xueguang Wang [a,*], Chunlei Zhang[b,*]

a State Key Laboratory of Advanced Special Steel, School of Materials Science and Engineering, Shanghai University, Shanghai 200072, China

b Technology Research Institute of Shanghai Huayi Group, Shanghai 200241, China

Keywords: Hydrogenation, Benzonitrile, Benzylamine, Pd/Al_2O_3, Alumina phases

* Corresponding author:

E-mail: wxg228@shu.edu.cn (X. G. Wang); zhangchunlei@shhuayi.com (C. L. Zhang)

Abstract:

Various phase alumina supports were prepared by heating commercial pseudoboehmite at 400 °C and 1200 °C to obtain gamma (γ) and alpha (α) Al_2O_3, and by calcinations of synthetic bayerite at 400 °C and 1000 °C to obtain Eta (η) and theta (θ) Al_2O_3. These supports were then impregnated and calcined to prepare 0.5 wt% Pd catalysts. The prepared catalysts were characterized by XRD, BET, NH_3–TPD, CO–TPD，H_2–TPR，etc., and their catalytic performances were evaluated for selective hydrogenation of benzonitrile. In the order of Pd/γ-Al_2O_3, Pd/η-Al_2O_3, Pd/θ-Al_2O_3 and Pd/α-Al_2O_3, the surface areas decreased from 265 to 3.8 m^2/g, the number of acidic sites was decreased, especially for strong acid sites, and meanwhile, the Pd size increased from 3.0 to 36.9 nm. The benzonitrile conversion showed limited relationship with the nature of catalysts and assumed to rely on the H_2 transmission rate. The dibenzylamine formation was considered to be a result of competitive reactions and performed as a function of the metal dispersion. Among the four Pd/Al_2O_3 catalysts, the Pd/γ-Al_2O_3 and Pd/η-Al_2O_3 both exhibited excellent stability and catalytic performance with a high benzylamine yield of ca. 90%.

1. Introduction

Benzylamine (BA) is an important chemical compound that has been found widespread applications in textile, chemical, military and agrochemical industries [1-8]. The heterogeneous catalytic hydrogenation of benzonitrile (BN) to benzylamine, regarded as having greater atom efficiency, is challenging due to undesired by-products including dibenzylamine (DBA), toluene (TOL), etc., as shown in Scheme 1 [9-11]. It is noteworthy that the byproduct DBA influences the product quality seriously, and it is recognized as being a priority to inhibit [12]. There has been much focus on the skeletal Ni [13] or Co [14] catalysts for their high activities to primary amines; however, considerable care is required in handling such pyrophoric catalysts on scale-up, and moreover, reactions often need to be carried out with vast amount of extra additives. Supported metal catalysts like Ir [15], Cu [16], Ru [17], Ni [18, 19] and Pd [11, 12, 20, 21], have been investigated for the hydrogenation of benzonitrile, and the Pd/Al_2O_3 catalysts exhibited the highest activity and selectivity [12]. Recently, we have investigated the Pd/Al_2O_3 catalyst systematically as well and found it superior in the trickle-bed hydrogenation of BN [22]. Over it, a long-term stability test was performed and deactivation study of corresponding Pd/Al_2O_3 catalyst indicated a transformation of the alumina phase during the running [23].

Support has been investigated in the hydrogenation of nitriles based on some traditional oxides, such as Al_2O_3, TiO_2, MgO and SiO_2 [24, 25]. These authors concentrated on the acid-base properties of these supports and considered that it was related to the selectivity of amines. However, in addition to the acid-base properties, the chemical properties of the supports might have a more pronounced effect on the catalytic performance. Hence, the usage of different crystalline alumina as supports will

be more convincing to understand the nature of supports on the catalytic performance, because they have the same chemical composition.

The crystal structure of support has been proved to play an interesting effect on the catalytic performance [26-28]. Hence, it is a desire to investigate the influence of alumina phases on the performance of Pd/Al_2O_3 catalyst in the hydrogenation of benzonitrile.

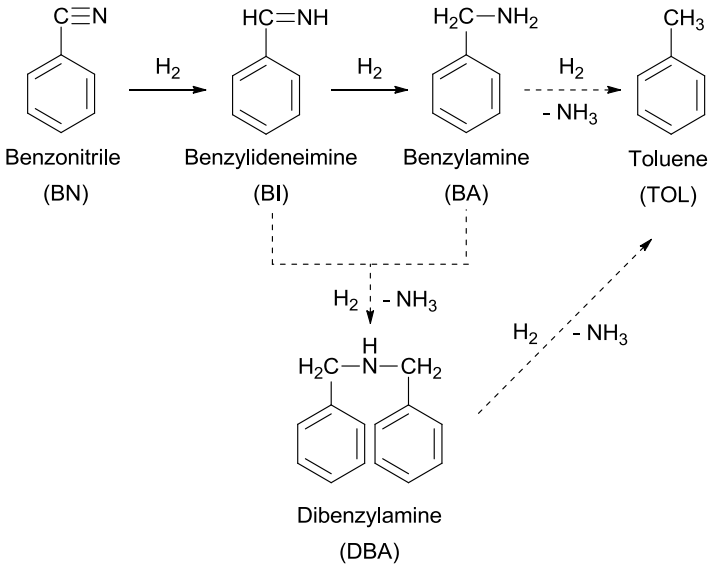

Scheme 1 Probable reaction pathways in the hydrogenation of benzonitrile to benzylamine.

2. Experimental

2.1 Catalysts preparation

Pseudoboehmite (AlO(OH), 413 m^2/g) and sodium aluminate ($NaAlO_2$) were obtained from CHALCO Shandong Co., Ltd. $Pd(NO_3)_2$ aqueous solution was purchased from Heraeus Materials Technology Shanghai Ltd. Other chemicals were graded analytically, purchased from Sinopharm Chemical Reagent Co., Ltd. and used without further purification.

The precursor, synthetic bayerite, was prepared by the following method similar to reported literature [29-31]. Initially, 250 mL of 2.4 mol/L $NaAlO_2$ aqueous solution were heated in a stainless steel batch reactor at 40 °C by a water bath. Then carbon dioxide was introduced and the pressure was increased to 1 MPa. With mechanical stirring, precipitate produced during the carbonation process was aged in the mother solution for 48 h. The resulting white precipitate was filtered and washed with distilled water as free as possible from alkali, then dried at 120 °C and was identified as $Al(OH)_3$ with crystal structure of bayerite, by powder X–ray diffraction (XRD), TG–DSC and FT–IR [31]. Eta (η) and theta (θ) phase alumina were obtained through calcinations of obtained bayerite at 400 °C and 1000 °C for 6 h, respectively. Similarly, gamma (γ) and alpha (α) phase alumina were obtained through calcinations of pseudoboehmite at 400 °C and 1200 °C for 6 h, respectively [32-35]. Various phase alumina synthesized above are characterized and identified as detailed below.

Various phase alumina supported Pd catalysts containing 0.5 wt% Pd were prepared through the incipient wetness impregnation of metal nitrates with above Al_2O_3 supports. As an example, 10 g of $Pd(NO_3)_2$ aqueous solution (0.047 mol/L, adjusted to pH of 1.5 by nitric acid) was dropped slowly into 10 g of γ-Al_2O_3 support (40–60 mesh) with vigorous mixing. The composites were aged at room temperature for 12 h, dried at 100 °C overnight and then calcined at 400 °C in air in a muffle furnace for 4 h. Then the fresh catalyst labeled Pd/γ-Al_2O_3 was obtained. The final Pd loadings of all supported catalysts were determined to be within the range of 0.47 ± 0.02 wt% by inductively coupled plasma optical emission spectrometry (ICP-OES).

2.2 Catalyst evaluation and analysis

Hydrogenation of benzonitrile was performed in a batch reactor at 90 °C under 1.5 MPa. The temperature was monitored by a thermocouple inserted in a thermowell within the solution. After filling the reactor with 1.25 g catalyst and 40 g ethanol, the system was purged with H_2 and pressurized to 1.5 MPa. Then, the solvent/catalyst mixtures were heated to 90 °C and kept for 2 h in order to reduce the catalyst under stirring at 1000 rpm [36]. 10 g BN was added to the batch reactor via a pressurized filling tank, in this way, the exact starting time of reaction could be assured. The ethanol serves as an inert solvent under reaction conditions. Samples were withdrawn periodically from the reaction mixture via an outlet valve and analyzed by Agilent 7890A equipped with a FID detector, employing a DB-5 capillary column. Benzonitrile conversion (X) and product selectivity (S_i) were calculated with the equation (Eqs. 1, 2), shown as follows:

$$\mathrm{X}(\%) = \frac{[BN]_{in} - [BN]_{out}}{[BN]_{in}} \times 100 \qquad (1)$$

$$\mathrm{S_i}(\%) = \frac{[\mathrm{Pr}oduct]_i \times \mathrm{N_i}}{[BN]_{in} - [BN]_{out}} \times 100 \qquad (2)$$

Where $[BN]_{in}$ and $[BN]_{out}$ are the molar amounts of BN in the inlet and outlet streams, respectively. $[Product]_i$ is the molar amounts of product i in the outlet mixture and N_i is the stoichiometric coefficient for product i with respect to BN, for example, the stoichiometric coefficient is 2 for DBA, and 1 for BA and TOL.

Turnover frequency (TOF) values are calculated by the formula as given below：

$$\mathrm{TOF} = \frac{\text{Reaction rate}}{\text{Number of Pd sites}}$$

Where reaction rate (mol/s) is calculated by the BN conversion within the initial reaction time of 15 min, and number of Pd sites (mol) is determined by CO chemisorption method.

2.3 Catalyst characterization

The X-ray diffraction (XRD) patterns were obtained at room temperature using Bruker D8-advance X-ray diffractometer. The powdered samples were scanned using Cu Kα radiation at a power of 40 kV and a current of 40 mA in the 2θ range of 10 – 80° with a scan rate of 2° per minute.

Thermogravimetry and differential scanning calorimeter measurements (TG – DSC) were performed with a simultaneous thermal analyzer model STA449F3 of NETZSCH Instruments. Non-isothermal experiments were carried out under dynamic conditions from room temperature to 1100 °C at a heating rate of 10 °C/min under air atmospheres. The average sample weight was about 30 mg, and the gas flow rate was 50 mL/min.

Fourier transform infrared (FT–IR) was carried on a Nicolet NEXUS 670 spectrometer with a resolution of 2 cm^{-1} using the KBr method.

Transmission electron microscopy (TEM) analyses were performed on a JEOL JEM-2100F microscope operating at 200 kV. The sample was prepared by placing a drop of ethanol solution of a well-ground catalyst powder onto a carbon-coated copper grid, followed by evaporation of ethanol.

N_2 adsorption and desorption isotherms were measured using a Quantachrome Autosorb–iQ analyzer at liquid nitrogen temperature (−196 °C). Prior to analysis, the sample was processed by vacuum degassing treatment for 16 h at 250 °C. The specific surface area (S_{BET}) was evaluated using the Brunauer–Emmett–Teller (BET) method in the P/P_0 range from 0.05 to 0.25. Pore size distribution curves were calculated using the desorption branch of the isotherms and the Barrett–Joyner–Halenda (BJH) method. Pore sizes were calculated by the BJH method and pore volumes were calculated from the adsorbed amount at $P/P_0 = 0.990$. The pore volume of Pd/α-Al_2O_3 was

measured by the water displacement method, and meanwhile, the average pore diameter was calculated from the pore volume and BET surface area data by assuming all pores have cylindrical shapes [37, 38]. In addition, the mesoporous structure of Pd/α-Al_2O_3 was also measured by a Quantachrome Poremaster-60 GT mercury porosimetry analyzer which provided the data of pore diameter and pore volume.

The temperature–programmed desorption of ammonia (NH_3–TPD) were conducted on a Micromeritics AutoChem II 2920 apparatus. Typically, about 50 mg sample was loaded in a quartz reactor and treated at 200 °C in He flow (30 mL/min) for 1 h, and then free cooled to 50 °C. Afterwards, the sample was pretreated with a 10 vol% NH_3/He mixed gas flow (30 mL/min) for 30 min and then purged in He flow (30 mL/min) for 60 min. Then the sample was heated to 800 °C at a rate of 10 °C/min with the flow of helium gas. Desorption of ammonia was monitored with a thermal conductivity detector (TCD).

Dispersion of metal Pd was determined by CO chemisorption on the same instrument as NH_3–TPD. About 50 mg sample was reduced in a 10 vol% H_2/He flow (30 mL/min) at 300 °C for 1 h, and then cooled to 50 °C and kept in a He flow (30 mL/min) for 30 min. After this, the sample was treated with a 10 vol% CO/He flow (30 mL/min) for 30 min, and then purged in flowing He (30 mL/min) for 60 min. The sample was heated to 600 °C at a rate of 10 °C/min in the He flow. The increase of the TCD signal area indicated the CO uptake chemisorbed. The metal dispersion (D) was calculated from the CO chemisorption data, where CO is known to adsorb on Pd in both an end-on configuration (CO/Pd = 1) and a bridged configuration (CO/Pd = 0.5) [39–42]. The configuration status are identified by the CO–TPD peak position and detailed in the text. The average particle size for reduced Pd^0 (d_{Pd}) was calculated by the equation of $d_{Pd} = 1.12/D$ (nm) [43, 44].

Temperature programmed reduction in hydrogen (H_2–TPR) was carried out on the same instrument as NH_3–TPD. About 50 mg sample was initially treated at 200 °C in He flow (30 mL/min) for 1 h and then cooled to 50 °C. Then a 10 vol% H_2/He mixture (30 mL/min) was admitted to the reactor and the sample was heated to 120 °C at a rate of 10 °C/min. H_2 consumption and evolution were measured with a TCD detector as a function of the temperature.

3. Result and discussion

3.1 Pseudoboehmite and bayerite

Pseudoboehmite used as the precursor to synthesize the γ- and α- phase Al_2O_3, was verified by XRD (see Fig. 1) [32]. The synthetic bayerite, applied for the synthesis of η- and θ- phase Al_2O_3, was identified by XRD, TG–DSC and FT–IR method, as shown in Fig. 2. The XRD result (Fig. 2a) showed the compounds were identified to $Al(OH)_3$ with primary crystal structure of bayerite according to JCPDS no. 74-1119. Fig. 2b showed the typical TG–DSC curves for the thermal decomposition of synthetic compound from room temperature to 1100 °C. The curves showed a sharp decomposition with a noticeable endothermic peak at ca. 255 °C, where the mass loss was ca. 30 wt%. These results were consistent with the theoretical value for the thermal decomposition of aluminum hydroxide to aluminum oxide, and were in good agreement with the data of bayerite in the reported literature [30, 31]. FT–IR spectra (Fig. 2c) verified the existence of crystalline bayerite. Five distinguished peaks due to O–H stretching vibration during 3400–3700 cm^{-1} were ascribed to the bayerite [30, 45]. In addition, O–H bending bands at 1024 and 974 cm^{-1} and a broad band centered at around 770 cm^{-1}, due to Al–OH group, were clearly observed for the composition. The IR spectrum of the crystallized compound was in good agreement with absorption

due to bayerite [29, 45]. The specific surface area of the sample was 9.1 m^2/g and the results are in good consistent with other studies [30, 46]. All in all, the synthetic compound was verified to be a relatively high purity bayerite.

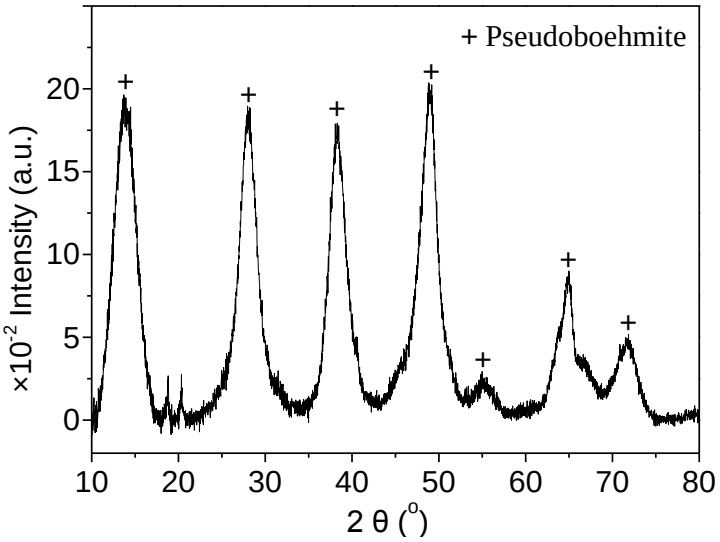

Fig. 1 XRD patterns of pseudoboehmite.

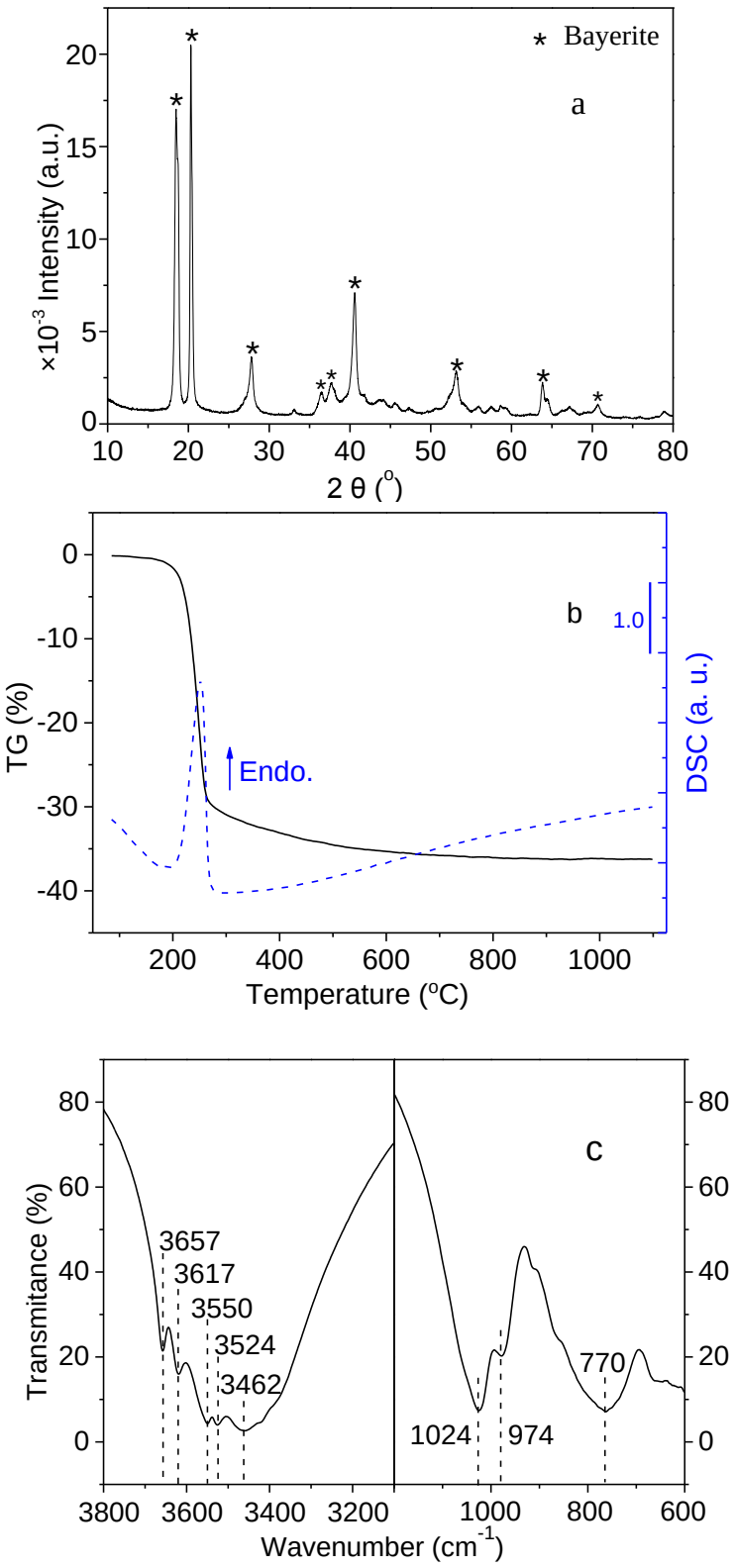

Fig. 2 Identification of synthetic bayerite. (a) XRD, (b) TG–DSC and (c) FT–IR.

3.2 Catalysts

3.2.1 XRD analysis

The XRD patterns of various phase alumina supported Pd catalysts were illustrated in Fig. 3. No diffraction peaks associated with Pd were observed in all cases due to the low loading and high dispersion of metal Pd.

Among the four Pd/Al_2O_3 catalysts, the θ-Al_2O_3 and α-Al_2O_3 supported catalysts exhibited characteristic XRD patterns which can be identified clearly according to JCPDS file no. 35–0121 for θ-Al_2O_3 and JCPDS file no. 10–0173 for α-Al_2O_3, respectively. The XRD patterns of the γ-Al_2O_3 and η-Al_2O_3 supported catalysts were very diffuse and exhibited extensive reflection overlapping. According to the method mentioned in other literatures, the γ and η alumina phases were distinguished through the comparison including the full width at half maximum (FWHM) of individual reflections with their hkl's and relative intensities [47, 48]. As a result, these samples were all proved to be well crystallized single-phase alumina and complied with the results in the literatures [28, 35, 47, 49].

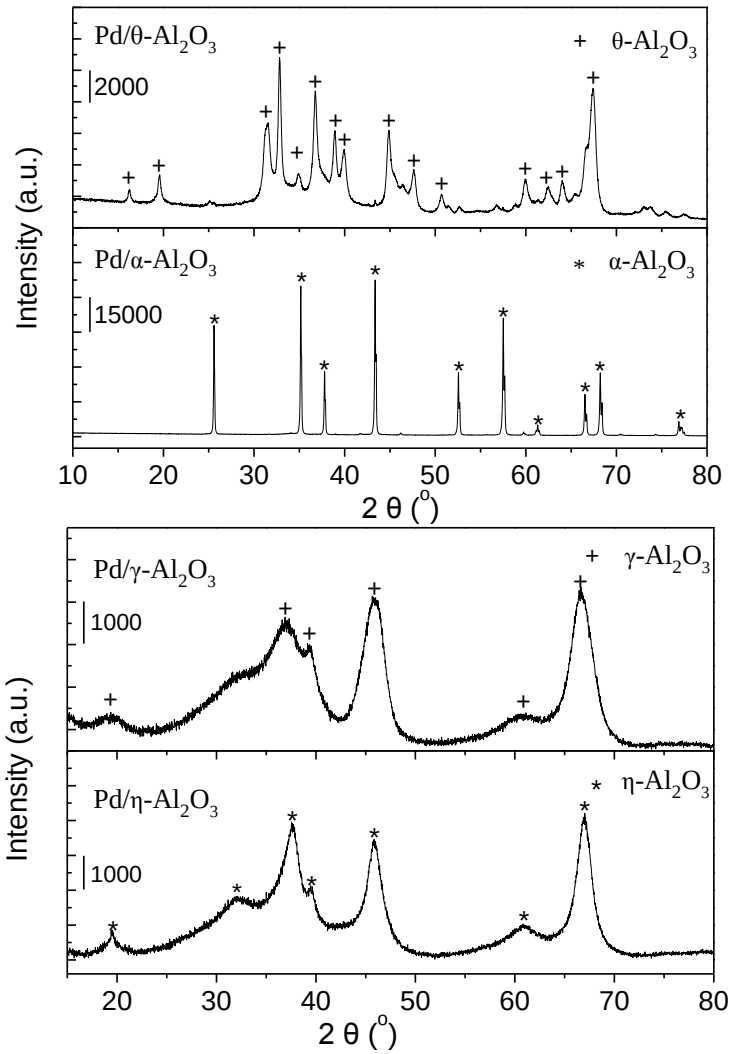

Fig. 3 XRD patterns of Pd/θ-Al_2O_3, Pd/α-Al_2O_3, Pd/γ-Al_2O_3 and Pd/η-Al_2O_3.

3.2.2 TEM analysis

As shown in Fig. 4a, b and c for γ-, η- and θ-Al_2O_3 supported catalysts, Pd particles could not be identified in the low magnification due to the low Pd loading and the interference of alumina supports. However, the presence of spherical Pd particles could be clearly evidenced by HR-TEM. The distance of 0.227 nm between the adjacent lattice fringes agreed well with the (1 1 1) lattice spacing of cubic metallic palladium nanoparticles [50, 51]. The sizes of Pd particles were located in the range of 3–8 nm, and increased gradually by the order of Pd/γ-Al_2O_3, Pd/η-Al_2O_3 and Pd/θ-Al_2O_3. In

Fig. 4d for Pd/α-Al_2O_3, the Pd particles exhibited obvious agglomeration. Similar results were also observed by other studies for Pd/α-Al_2O_3 [52]. The mean sizes of Pd particles were listed in the following Table 2 for convenient comparison.

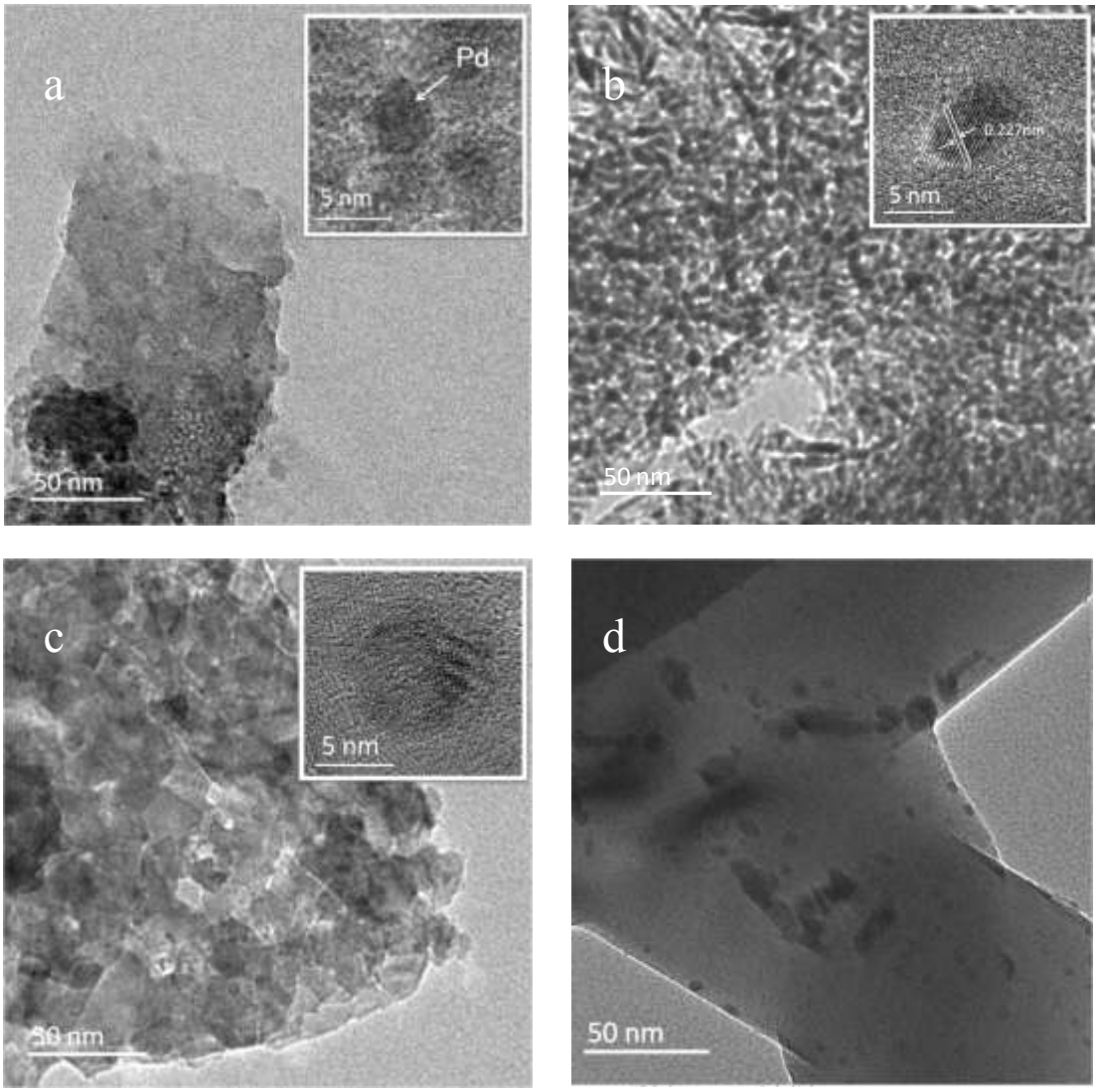

Fig. 4 TEM images of the reduced Pd/Al_2O_3 catalysts: (a) Pd/γ-Al_2O_3, (b) Pd/η-Al_2O_3, (c) Pd/θ-Al_2O_3 and (d) Pd/α-Al_2O_3.

3.2.3 Textural properties

The specific surface areas, pore volumes, and average pore diameters of the support precursors and the Pd/Al_2O_3 catalysts are given in Table 1. Due to the low Pd loading, the textural properties of catalysts are ascribed to the nature of supports itself.

Compared with pseudoboehmite, Pd/γ-Al_2O_3 and Pd/α-Al_2O_3 showed an apparent decrease in surface area and pore volume, which could be attributed to particle sintering and structure collapse during calcination [53]. Considering the fact that the calcination temperature of Pd/α-Al_2O_3 is up to 1200 °C and the specific surface area is only 3.8 m^2/g, Pd/α-Al_2O_3 has scarcely pore structure. On the contrary, Pd/η-Al_2O_3 and Pd/θ-Al_2O_3 exhibited porous structures while its precursor, namely the bayerite, has low surface area of 9.1 m^2/g and small pore volume. It might be caused by the reaming effects in the dehydration process of bayerite during calcination.

The pore size distributions of the Pd/Al_2O_3 catalysts are illustrated in Fig. 5. A single pore structure was observed for Pd/γ-Al_2O_3 and Pd/η-Al_2O_3 except the latter showed a much narrower pore size distribution. The Pd/θ-Al_2O_3 exhibited broad pore size distribution with large pore size, indicating the poor pore structure originated from the accumulation of particles.

Table 1 Textural properties of the precursors and Pd/Al_2O_3 catalysts.

Samples	S_{BET} (m^2/g)	Pore diameter (nm)	Pore volume (cm^3/g)
Pseudoboehmite	413	5.2	0.45
Bayerite	9.1	24.9	0.06
Pd/γ-Al_2O_3	265	9.9	0.68
Pd/η-Al_2O_3	256	5.3	0.30
Pd/θ-Al_2O_3	55.3	22.9	0.32
Pd/α-Al_2O_3	3.8	147[b] / 241[c]	0.14[a] / 0.16[c]

a Measured by the water displacement method.

b Average pore diameter = (4×pore volume) / (BET surface area), by assuming all pores have cylindrical shapes.

c Measured by a mercury porosimeter.

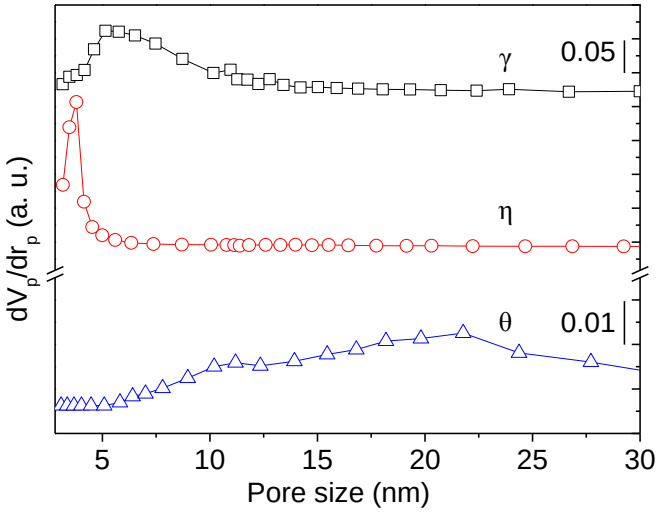

Fig. 5 BJH pore size distributions of the Pd/Al_2O_3 catalysts.

3.2.4 NH_3–TPD analysis

The NH_3–TPD profiles in Fig. 6 indicate the acidity of the Pd/Al_2O_3 catalysts decreased in the order of γ-Al_2O_3 > η-Al_2O_3 > θ-Al_2O_3 > α-Al_2O_3 by the supports. The tendency was approximately consistent with the increasing calcination temperature of supports due to the continuous dehydration at higher temperature. The γ and η phase alumina were calcined at the same temperature and both of them showed large amounts of weak and strong acidic positions. However, because of the different structure or type of precursor being considered possibly, γ-Al_2O_3 showed a greater numbers of the acid sites than that of η-Al_2O_3. The results were in good agreement with the report by D.S. Maciver [49], who found the water content of γ-Al_2O_3 was much greater than that of η-Al_2O_3 and showed higher acidity. As a complete dehydration product, the α-Al_2O_3 had rarely acidic positions.

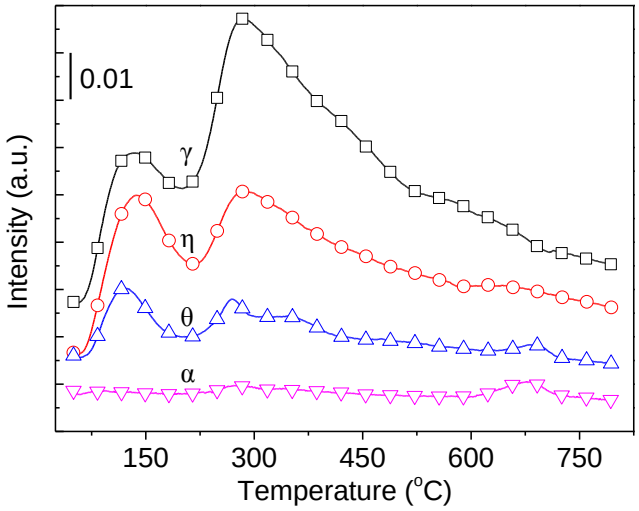

Fig. 6 NH_3–TPD profiles of the Pd/Al_2O_3 catalysts.

3.2.5 CO–TPD analysis

The CO–TPD profiles of various catalysts are illustrated in Fig. 7. The CO adsorption results, Pd dispersions and the average Pd metal particle sizes determined from CO chemisorption are given in Table 2. The CO desorption curves indicate a diversity of adsorption sites for CO on Pd as well as variation in the proportion and distribution of CO species. $Pd/\gamma\text{-}Al_2O_3$ and $Pd/\eta\text{-}Al_2O_3$ catalysts showed similar behavior with three peaks at ca. 88, 173 and 410 °C, except for the $Pd/\eta\text{-}Al_2O_3$ catalyst the desorption of these peaks were slightly shifted to higher temperatures. The $Pd/\theta\text{-}Al_2O_3$ catalyst exhibited a single peak at ca. 135 °C, whereas $Pd/\alpha\text{-}Al_2O_3$ catalyst showed only tiny desorption. As indicated by Monteiro et al. [54], the two peaks (L1, L2) at low temperatures (<300 °C) were attributed to linearly-bonded CO on Pd (1 0 0) and Pd (1 1 1) planes, respectively, and the peak (B) at high temperature (>300 °C) was assigned to bridged–bonded CO on Pd (1 1 1) plane. The distribution of these species changed as supports change (Table 2). Where, in the order of $Pd/\gamma\text{-}Al_2O_3$, $Pd/\eta\text{-}Al_2O_3$, $Pd/\theta\text{-}Al_2O_3$ and $Pd/\alpha\text{-}Al_2O_3$, the molar ratio of bridge to linear (B/L) and L2 to L1

(L2/L1) decreased sharply, reveals the transformation from strongly adsorbed species to weakly adsorbed ones.

The mean diameters of Pd particles determined by CO chemisorptions in Table 2 are about 3.0, 5.3 8.5 and 36.9 nm for Pd/γ-Al_2O_3, Pd/η-Al_2O_3, Pd/θ-Al_2O_3 and Pd/α-Al_2O_3, respectively. These values are consistent with the sizes of Pd particles by TEM shown in Table 2.

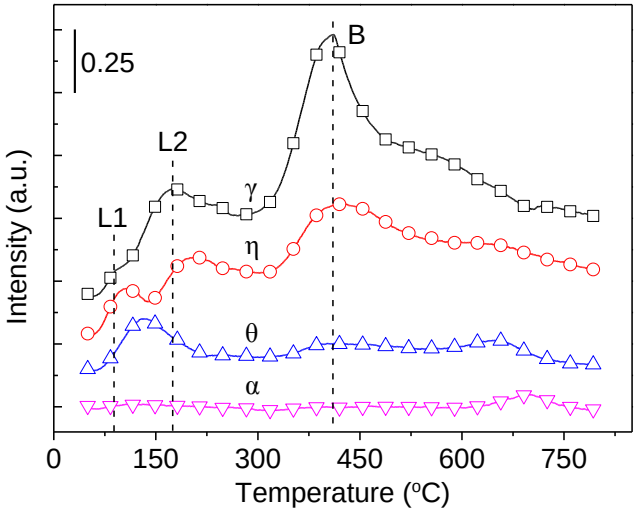

Fig. 7 CO–TPD profiles of the Pd/Al_2O_3 catalysts.

Table 2 CO chemisorption results of the Pd/Al_2O_3 catalysts.

Catalysts	CO linear[a] (μmol/g)		L2/L1 ratio	CO bridged[b] (μmol/g)	B/L ratio[c]	Pd dis-persion (%)	Pd particle size (nm)	
	L1	L2		B			d_{CO}	d_{TEM}
Pd/γ-Al_2O_3	0.11	1.8	17.0	7.8	4.1	37.4	3.0	3.5±1.2
Pd/η-Al_2O_3	0.31	1.2	4.0	4.2	2.7	21.1	5.3	4.8±1.6
Pd/θ-Al_2O_3	1.4	–	–	2.4	1.7	13.6	8.5	8.0±3.0
Pd/α-Al_2O_3	–	–	–	0.7	–	3.0	36.9	32±18

[a] L1 and L2 are the linearly bonded CO, respectively.

[b] B is the bridged-bonded CO.

[c] L = L1 + L2.

3.2.6 H_2–TPR analysis

The TPR curves of the catalysts are shown in Fig. 8, where no consumption peaks were observed in all cases due to the fact that PdO can be reduced below 20 ºC [55, 56]. Except for the Pd/γ-Al_2O_3, all the other three catalysts exhibited a negative H_2 peak at around 65 ºC. This peak is attributed to the H_2 desorption from the decomposition of β–PdH formed at room temperature (5 min) before the start of TPR run [57-60]. The formation of β–PdH depends on the particle size of palladium; larger Pd particles more easily form β–PdH phase, whereas smaller Pd particles may be unable to form the Pd hydride [59, 61]. Some studies indicated the critical size of crystallite Pd is 2–3 nm [39, 54] which are in good agreement with the catalysts behavior in this study. Furthermore, the β–PdH decomposition peak of Pd/α-Al_2O_3 shifted to higher temperatures and the area decreased 25% by compared with that of Pd/θ-Al_2O_3. The reason may lie in the inadequate reaction of bulk palladium and its lag during the decomposition of β–PdH phase.

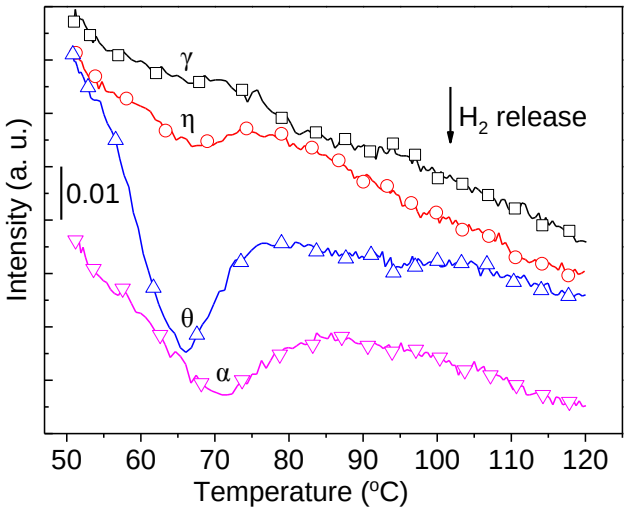

Fig. 8 H_2–TPR profiles of the Pd/Al_2O_3 catalysts.

3.3 Catalytic performance

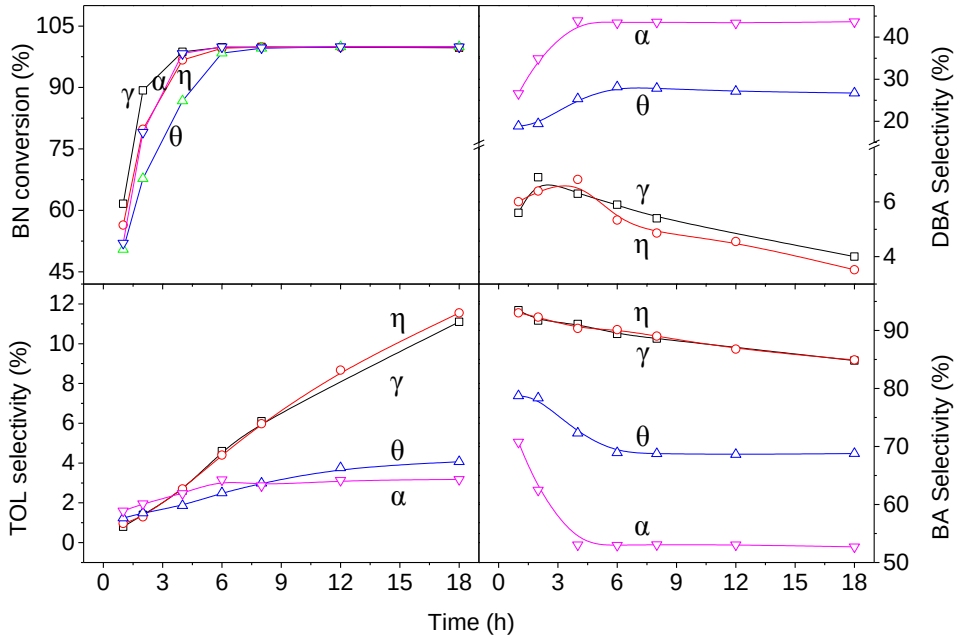

Fig. 9 Catalytic performance of Pd/Al_2O_3 catalysts as a function of reaction time.

Table 3 Catalytic reaction rate and TOF values of the Pd/ Al_2O_3 catalysts.

Samples	Reaction rate[a] (10^{-3} g/s $g_{catalyst}$)	TOF (s^{-1})
Pd/γ-Al_2O_3	1.4	0.8
Pd/η-Al_2O_3	1.3	1.4
Pd/θ-Al_2O_3	1.1	2.0
Pd/α-Al_2O_3	1.3	9.7

[a] BN consumption rate based on the initial 15 min results.

For the comparison of these catalysts supported on different phase alumina, contrast tests are carried out in a batch reactor under the same conditions. Comparative results including the BN conversion and product selectivity (DBA, TOL and BA) are demonstrated in Fig. 9. The curves of BN conversions for the four catalysts are similar and they all reached total conversion after 6 h.

Table **3** listed the initial catalytic activities and corresponding TOF values. The initial BN conversion rate are all in the range of 1.1-1.4 $\times 10^{-3}$ g/s $g_{catalyst}$ and the Pd/α-Al_2O_3 with the minimum surface area and the maximum Pd particle size exhibited close performance with other catalysts. However, the TOF values showed a significant difference over these catalysts, which varied from 0.8 to 9.7 s^{-1}. Considering the similar Pd loading and identical preparation methods of these catalysts, these results all implied the BN conversion has no direct relationship with the surface area, supports acidity, or the metal dispersion. The reason can be explained as that in our previous work [22], that the terrible hydrogenation transmission is regarded as the limiting step in batch reactor and plays a key role on the BN conversion. As a result, the conversion of BN relied on the H_2 transmission rate rather than the nature of catalysts itself.

Concerning the condensation by-product DBA formation, the plots of the DBA selectivity showed that the weaker acidity of the catalyst, the higher DBA selectivity was achieved. It is opposite to conventional belief that DBA formation could be accelerated by acidic sites. The results inferred that the condensation reactions proceed with no participation of the support and in agreement with other reports [62, 63]. The behavior of the DBA selectivity for the four catalysts was considered to be a result of competitive reactions. As shown in Scheme 1, DBA is formed via a condensation reaction which relies on the amounts of semi-hydrogenated intermediate of BN. Larger particle size, or lower metal dispersion, can reduce the activity of the catalyst. It promoted the formation of intermediate products instead of the hydrogenolysis to toluene, and thus enhanced the DBA formation [22]. Hence, the DBA selectivity performed as a function of the catalyst activity which mainly related to the metal dispersion. Furthermore, the DBA selectivity for Pd/γ-Al_2O_3 and Pd/η-Al_2O_3 decreases gradually

with the reaction time after reaching a peak value at 3 h. In consideration of other products, a further hydrogenolysis and deamination of DBA and BA are carried out and generate TOL over them. The behavior did not appear on the Pd/θ-Al_2O_3 and Pd/α-Al_2O_3 catalysts. Their DBA selectivity climbed up and remained stable as a function of reaction time, indicating the hydrogenation of BN over these catalysts was weakened, and most likely, the catalysts were deactivated.

Overall, among the four Pd/Al_2O_3 catalysts, the Pd/γ-Al_2O_3 and Pd/η-Al_2O_3 catalysts both exhibited excellent selectivity of BA at high activity with the extremely lower DBA selectivity, and simultaneously, a high BA yield up to 90% was achieved over them, which was superior to that in other literatures [21, 39].

4. Conclusions

Different transition alumina including γ, η, θ and α phase alumina, were prepared by calcinations of commercial pseudoboehmite and synthetic bayerite. These supports were then impregnated and calcined to prepare 0.5 wt% Pd catalysts. The prepared catalysts were characterized by XRD, BET, NH_3–TPD, CO–TPD，H_2–TPR，etc., and showed different active sites, dispersion and adsorption strength. Their catalytic performances were evaluated for selective hydrogenation of benzonitrile. The BN conversion showed no direct relationship with the nature of catalysts and assumed to be relied to the H_2 transmission rate. The DBA formation was considered to be a result of competitive reactions and performed as a function of the metal dispersion. Among the four Pd/Al_2O_3 catalysts, the Pd/γ-Al_2O_3 and Pd/η-Al_2O_3 both exhibited excellent stability and catalytic performance with high BA yield of ca. 90%.

Reference

[1] P. Morieux, J.P. Stables, H. Kohn, Biorg. Med. Chem. 16 (2008) 8968-8975.

[2] U.R. Nair, R. Sivabalan, G.M. Gore, M. Geetha, S.N. Asthana, H. Singh, Combustion, Explosion and Shock Waves. 41 (2005) 121-132.

[3] G.V. Lommen, M. De Bruyn, M. Schroven, W. Verschueren, W. Janssens, J. Verrelst, J. Leysen, Bioorg. Med. Chem. Lett. 5 (1995) 2649-2654.

[4] S. Nishimura, Handbook of heterogeneous catalytic hydrogenation for organic synthesis, John Wiley & Sons, New York (2001).

[5] H.-U. Blaser, C. Malan, B. Pugin, F. Spindler, H. Steiner, M. Studer, Adv. Synth. Catal. 345 (2003) 103-151.

[6] S.A. Lawrence, Amines: Synthesis, Properties and Application, Cambridge University Press, Cambridge (2004).

[7] H.A. Wittcoff, B.G. Reuben, J.S. Plotkin, Industrial Organic Chemicals, John Wiley & Sons, Inc. (2005) 15-56.

[8] D. Choi, J.P. Stables, H. Kohn, J. Med. Chem. 39 (1996) 1907-1916.

[9] D.B. Bagal, B.M. Bhanage, Adv. Synth. Catal. 357 (2015) 883-900.

[10] H. Yoshida, Y. Wang, S. Narisawa, S.-i. Fujita, R. Liu, M. Arai, Appl. Catal., A. 456 (2013) 215-222.

[11] M. Chatterjee, H. Kawanami, M. Sato, T. Ishizaka, T. Yokoyama, T. Suzuki, Green Chem. 12 (2010) 87-93.

[12] Y. Hao, M. Li, F. Cárdenas-Lizana, M.A. Keane, Catal. Lett. 146 (2016) 109-116.

[13] Y. Hao, Palladium and gold catalysts for sustainable chemical processing, Doctor thesis, School of Engineering and Physical Sciences, Heriot-Watt University (2015).

[14] P. Schärringer, Kinetic and mechanistic studies on the liquid-phase hydrogenation of nitriles and dinitriles over cobalt-based catalysts, Doctor thesis, University of Munich, (2007).

[15] Y.M. López-De Jesús, C.E. Johnson, J.R. Monnier, C.T. Williams, Top. Catal. 53 (1994) 1132-1137.

[16] R.K. Marella, K.S. Koppadi, Y. Jyothi, K.S. Rama Rao, D.R. Burri, New J. Chem. 37 (2013) 3229-3235.

[17] C. de Bellefon, P. Fouilloux, Cat. Rev. - Sci. Eng. 36 (1994) 459-506.

[18] D.J. Ostgard, Spec. Chem. Mag. 28 (2008) 28-31.

[19] S.P. Bawane, S.B. Sawant, Chem. Eng. J. 103 (2004) 13-19.

[20] A.J. Yap, A.F. Masters, T. Maschmeyer, ChemCatChem. 4 (2012) 1179-1184.

[21] L. Hegedűs, T. Máthé, Appl. Catal., A. 296 (2005) 209-215.

[22] C. Dai, S. Zhu, X. Wang, C. Zhang, W. Zhang, Y. Li, C. Ning, New J. Chem. (2017).

[23] C. Dai, F. Liu, W. Zhang, Y. Li, C. Ning, X. Wang, C. Zhang, Appl. Catal., A. 538 (2017) 199-206.

[24] C.V. Rode, M. Arai, M. Shirai, Y. Nishiyama, Appl. Catal., A. 148 (1997) 405–413.

[25] M.J.F.M. Verhaak, A.J.V. Dillen, J.W. Geus, Catal. Lett. 26 (1994) 37-53.

[26] T. Glinrun, O. Mekasuwandumrong, J. Panpranot, C. Chaisuk, P. Praserthdam, Reac Kinet Mech Cat. 100 (2010) 441-448.

[27] C. Meephoka, C. Chaisuk, P. Samparnpiboon, P. Praserthdam, Catal. Commun. 9 (2008) 546-550.

[28] D.S. MacIver, W.H. Wilmot, J.M. Bridges, J. Catal. 3 (1964) 502-511.

[29] T. Sato, T. Yamashita, F. Ozawa, Z. Anorg. Allg. Chem. 370 (1969) 202-208.

[30] N. Koga, T. Fukagawa, H. Tanaka, J. Therm. Anal. Calorim. 64 (2001) 965-972.

[31] N. Koga, Solid State Ionics. 172 (2004) 253-256.

[32] G. Toledo-Chávez, J.-C. Paniagua-Rodríguez, J. Zárate-Medina, R. Maya-Yescas, Catal. Today. 271 (2016) 207-212.

[33] L. Favaro, A. Boumaza, P. Roy, J. Lédion, G. Sattonnay, J.B. Brubach, A.M. Huntz, R. Tétot, J. Solid State Chem. 183 (2010) 901-908.

[34] A. Boumaza, L. Favaro, J. Lédion, G. Sattonnay, J.B. Brubach, P. Berthet, A.M. Huntz, P. Roy, R. Tétot, J. Solid State Chem. 182 (2009) 1171-1176.

[35] I. Levin, D. Brandon, J. Am. Ceram. Soc. 81 (1998) 1995-2012.

[36] L. McMillan, L.F. Gilpin, J. Baker, C. Brennan, A. Hall, D.T. Lundie, D. Lennon, J. Mol. Catal. A: Chem. 411 (2016) 239-246.

[37] M. Takht Ravanchi, M. Rahimi Fard, S. Fadaeerayeni, F. Yaripour, Chem. Eng. Commun. 202 (2014) 493-499.

[38] Y.-W. Rhee, J.A. Guin, Korean J. Chem. Eng. 10 (1993) 112-123.

[39] J.J.W. Bakker, A.G.v.d. Neut, M.T. Kreutzer, J.A. Moulijn, F. Kapteijn, J. Catal. 274 (2010) 176-191.

[40] C. Amorim, M.A. Keane, J. Colloid Interface Sci. 322 (2008) 196-208.

[41] G. Fagherazzi, A. Benedetti, S. Polizzi, A. Mario, F. Pinna, M. Signoretto, N. Pernicone, Catal. Lett. 32 (1995) 293-303.

[42] J. Sa, G.D. Arteaga, R.A. Daley, J. Bernardi, J.A. Anderson, J. Phys. Chem. B 110 (2006) 17090-17095.

[43]M. Martin-Martinez, L.M. Gómez-Sainero, M.A. Alvarez-Montero, J. Bedia, J.J. Rodriguez, Appl. Catal., B. 132-133 (2013) 256-265.

[44]N. Mahata, V. Vishwanathan, J. Catal. 196 (2000) 262-270.

[45]H.D. Ruan, R.L. Frost, J.T. Kloprogge, J. Raman Spectrosc. 32 (2001) 745-750.

[46]X. Du, X. Su, Y. Wang, J. Li, Mater. Res. Bull. 44 (2009) 660-665.

[47]R.S. Zhou, R.L. Snyder, Acta Crystallogr. Sect. B: Struct. Sci. 47 (1991) 617-630.

[48]M.F. Fisher, D. White, J. Mater. Sci. 11 (1976) 1165-1167.

[49]D.S. Maciver, H.H. Tobin, R.T. Barth, J. Catal. 2 (1963) 485-497.

[50] J. Hu, Z. Zhou, R. Zhang, L. Li, Z. Cheng, J. Mol. Catal. A: Chem. 381 (2014) 61-69.

[51] D. Berger, G.A. Trăistaru, B.S. Vasile, I. Jitaru, C. Matei, UPB Bul. Stiint. Ser. B: Chem. Mater. Sci. 72 (2010) 113-120.

[52] D. Nagai, M. Nishibori, T. Itoh, T. Kawabe, K. Sato, W. Shin, Sensor Actuat B-Chem. 206 (2015) 488-494.

[53]S. Komeili, M.T. Ravanchi, A. Taeb, Appl. Catal., A. 502 (2015) 287-296.

[54]R.S. Monteiro, L.d.C. Dieguez, M. Schmal, Catal. Today. 65 (2001) 77-89.

[55] C. Neyertz, M.A. Volpe, C. Gigola, Catal. Today. 57 (2000) 255-260.

[56]C. Neyertz, M. Volpe, Colloids Surf Physicochem Eng Aspects. 136 (1998) 63-69.

[57]C.M. Mendez, H. Olivero, D.E. Damiani, M.A. Volpe, Appl. Catal., B. 84 (2008) 156-161.

[58]N.S. Babu, N. Lingaiah, R. Gopinath, P.S. Sankar Reddy, P.S. Sai Prasad, J. Phys. Chem. C. 111 (2007) 6447-6453.

[59]J. Panpranot, O. Tangjitwattakorn, P. Praserthdam, J.G. Goodwin, Appl. Catal., A. 292 (2005) 322-327.

[60]J. Panpranot, K. Pattamakomsan, P. Praserthdam, J.G. Goodwin, Ind. Eng. Chem. Res. 43 (2004) 6014-6020.

[61]B. Coq, S. Hub, F. Figuéras, D. Tournigant, Appl. Catal., A. 101 (1993) 41-50.

[62]S. Gomez, J.A. Peters, T. Maschmeyer, Adv. Synth. Catal. 344 (2002) 1037-1057.

[63]J. Krupka, J. Pasek, Curr. Org. Chem. 16 (2012) 988-1004.